© 2016 IJSRST | Volume 2 | Issue 1 | Print ISSN: 2395-6011 | Online ISSN: 2395-602X
Themed Section: Science and Technology

Influence of Electro Discharge Machining, Micro Structural and Mechanical Properties on Wear Behaviour of WC-30%Co Composites

D. Kanagarajan
Department of Manufacturing Engineering, Annamalai university, Annamalai Nagar, Tamil Nadu, India
Email : mfgkanagaraj@gmail.com

ABSTRACT

WC-Co hard metals are composite materials. They have very good properties like high hardness and relatively high fracture toughness. They offer high resistance to wear and rupture strength. They are used in cutting tools industry and other applications like mining, metal forming, construction industry, wear parts etc.-Co contains classic composition of WC and Co. The WC grains provide high hardness and wear resistance and the cobalt binder increases toughness. The vast majority of applications for tungsten carbide cobalt (WC–Co) composites exploit its high resistance to wear when subjected to abrasion and erosion and thus, an understanding of its response to tribological environments has major commercial implications. However, the conventional machining of this material is difficult hence the EDM is used for machining of this composite material. The present study focuses to develop wear transition maps and wear mechanism maps for the surface of WC-Co composite material produced through powder metallurgy route and also compare the same composition of the EDMedsurfaces. Wear maps can be constructed systematically by using consistent database, once constructed will provide a material selection guide as well as a design guide for an engineering application. One can also classify the wear processes by using the wear map approach which allows one to conduct critical experiments in the right combination of material, operating condition, and environment to investigate the different wear mechanisms. In conventional empirical wear mechanism maps, it is difficult to establish the boundaries of different mechanisms. Hence it is decided to use probabilistic neural networks (PNN) to develop the wear mechanism maps.

Keywords : Tungsten Carbide Cobalt (WC/Co) Composites, EDM, PNN

I. INTRODUCTION

The EDM process can be compared with the conventional cutting process, except that in the case, a suitably shaped tool electrode, with a precision-controlled feed movement is employed in place of the cutting tool, and the cutting energy is provided by means of short duration electrical impulses. EDM has found ready application in the machining of hard metals or alloys, which cannot be machined easily by conventional methods. It thus plays a major role in the machining of dies, tools, etc.[1,2]. It is thermal in nature with material removal occurring via the discharge of energy between a tool and work piece electrode, which are separated by a small gap (5-100μs), followed by a similar period during which deionization of the dielectric occurs and the gap is flushed of debris [3].Basic characteristics required for the dielectric used in EDM are high dielectric strength and quick recovery after breakdown, effective quenching and flushing ability. Besides these basic requirements, practical criteria to be considered in the selection of a dielectric include health and safety, maintenance, and cost. Tool wear and metal removal.

Dielectric flushing methods can be broadly divided into four main categories: normal flow, reverse flow, jet flushing and immersion flushing. In normal flow, the dielectric fluid is fed through the tool or work

piece and exits through the gap, and as the name implies, in the case of reverse flow, the flow is reversed by drawing the dielectric away from the gap instead. Flow conditions may be unstable with reduced removal rate and uneven tool wear. The flow velocity can be monitored by measuring the differential pressure or volume throughout. In jet flushing, a continuous jet of dielectric is directed at the gap, is used in die sinking EDM or machining of narrow slots and cavities

WC-Co hard metals are composite materials. They have very good properties like high hardness and relatively high fracture toughness. They offer high resistance to wear and rupture strength. They are used in cutting tools industry and other applications like mining, metal forming, construction industry, wear parts etc. Use of these hard metals leads to reduced cost and improved tool life comparing to conventional high-speed steel tools. WC-Co contains classic composition of WC and Co. The WC grains provide high hardness and wear resistance and the cobalt binder increases toughness. The question of great practical importance is, how much of the material will be lost during the given operating time. The surface shapes vary due to their functions, manufacturing tolerances, etc. and will be changed as a result of wear and plastic deformation [4].The vast majority of applications for tungsten carbide cobalt (WC–Co) composites exploit its high resistance to wear when subjected to abrasion and erosion and thus, an understanding of its response to tribological environments has major commercial implications. However, the development of such an understanding is complicated by the fact that as a composite material WC–Co displays properties, which vary over a particularly wide range and are strongly dependent on its microstructural parameters [5].

Wear maps can be constructed systematically by using consistent database, once constructed will provide a material selection guide as well as a design guide for an engineering application. One can also classify the wear processes by using the wear map approach which allows one to conduct critical experiments in the right combination of material, operating condition, and environment to investigate the different wear mechanisms.

The wear maps are used in normal practice to identify and predict the wear behavior of one material sliding against another at different sliding conditions [6]. The ability to predict wear of materials is a universal challenge crucial to successful application of new materials into different technologies, from nanometer scale to micrometer scale. As more and more new materials become available, design guideline of these new materials in a comprehensive manner to predict performance and lifetime take on additional urgency. Wear of a material is dependent on different parameters such as contact geometry, surface roughness, micro structural features, grain size, fracture toughness, speed, load, temperature, duration, environment, lubrication, etc.[7].

Wear mechanism map not only provides a multi objective graphical presentation of wear data, it also provides an overall framework for the wear behavior of a particular sliding system in which individual wear mechanisms can be observed under various sliding (operating) conditions. Many names have been given to diagrams, which describe the overall behavior of wear, the more commonly used are wear mechanism map, wear mode map, wear transition map and wear regime map. Generally, wear mode, wear transition and wear regime maps tend to focus on the description of the mode of wear, namely, mild wear, severe wear and ultra-severe wear and the transition between them. In the case of wear mechanism maps, details of the dominant wear mechanisms are given and the regions of their dominance are indicated[8].

The present study focuses to develop wear transition maps and wear mechanism maps for the surface of different compositions of WC-Co composite material produced through powder metallurgy route and also compare the same composition of the EDMed surfaces. In conventional empirical wear mechanism maps, it is difficult to establish the boundaries of different mechanisms. Hence it is decided to use probabilistic neural networks (PNN) to develop the wear mechanism maps.

II. EXPERIMENTAL WORK

A. Specimen preparation and Wear Testing

The dies and punches used should be highly polished and the clearance between them should be kept at the minimum for proper alignment. Clearance should be sufficient to allow a free movement. Hydraulic press are best suited for high pressures and for parts of uniform density. In this research the 150-ton capacity hydraulic press is used for producing green compacts of tungsten carbide and cobalt composites. The hydraulic press in pressing action of with cylindrical die is shown in Figure1The usual sequence of operations in die compacting include filling of die cavity with a definite volume of WC/Cobalt powder, application of the required pressure by movement of the upper and lower punches towards each other, and finally ejection of the green compacts by the lower punch. The pressure applied ranged from 650-750MPa depending on the composition.

Figure 1: 150-Ton Hydraulic press

Figure 2: Wear specimen

Figure 3: EDMed wear specimen

Wear is a complex phenomenon. It occurs whenever surfaces come into sliding contact, even in the presence of lubricant. The study of this phenomenon plays a vital role in designing any component of longer endurance. Wear tests are carried out in dry sliding conditions. The tests are performed using a pin-on ring type wear apparatus. Wear test samples in the form of pins (φ12mmX12mm) are produced through powder metallurgy route. The most important operation of powder metallurgy is compacting or pressing. It is a process of converting loose powder in to a green compact of accurate shape and size. It is done in high carbon high chromium steel dies and punches.

The surfaces are prepared by grinding the surfaces manually using 240, 320, 400 and 600 grit SiC papers. The face of the specimen is pressed against with the slider ring. The counter face ring is made of AISI 52100 type bearing steel covered with 200 grit alumina sheets. The width of the ring used is 12mm. The tests are carried out at a sliding velocity range of 0.1 to 2.0m/s and the load range used is between 1 to 350 N. Loss of mass from the surfaces of specimens are determined as a function of sliding distance at each load using different sliding conditions. The interfacial temperature is measured using thermocouple attachments.

The mass losses are calculated from the difference in weight of specimens measured before and after the sliding tests (after removing any loose debris) to the nearest 0.lmg using an analytical balance. Volumetric wear loss is estimated by dividing the mass loss by the density of work material. The normalised velocity, force and wear rate are obtained using the following relations [9]. The wear test experiments are conducted inWC-30Co composites of before and after EDMed surfaces. The EDM parameters used for the testing include C=15A, S=814rpm, T=200μs and P=1.5Kg/cm^2. The parameters are obtained through optimization (NSGA-II) to give optimum level of MRR and Ra

TABLE I. Wear rate for as produced WC-30Co composite

S.No	Normalized velocity	Normalized pressure	Wear rate
1.	0	-8	$10^{-9.0}$
		-7	$10^{-8.0}$
		-6	$10^{-7.0}$
		-5	$10^{-6.0}$
		-4	$10^{-5.5}$
		-3	$10^{-5.0}$
		-2	$10^{-4.0}$
		-1	$10^{-3.5}$
		0	$10^{-3.0}$
		-8	$10^{-6.0}$
		-7	$10^{-5.5}$
		-6	$10^{-5.4}$
		-5	$10^{-5.3}$
		-4	$10^{-5.0}$
2.	1	-3	$10^{-4.3}$
		-2	$10^{-4.0}$
		-1	$10^{-3.8}$
		0	$10^{-3.0}$
		-8	$10^{-5.0}$
		-7	$10^{-4.5}$
		-6	$10^{-4.0}$
		-5	$10^{-3.8}$
3.	2	-4	$10^{-3.5}$
		-3	$10^{-3.4}$
		-2	$10^{-3.3}$
		-1	$10^{-3.1}$
		0	$10^{-2.9}$
		-8	$10^{-4.0}$
		-7	$10^{-3.8}$
		-6	$10^{-3.5}$
		-5	$10^{-3.4}$
		-4	$10^{-3.2}$
4.	3	-3	$10^{-3.1}$
		-2	$10^{-3.0}$
		-1	$10^{-2.0}$
		0	$10^{-1.0}$
		-8	$10^{-4.0}$
		-7	$10^{-3.8}$
		-6	$10^{-3.5}$
		-5	$10^{-3.4}$
		-4	$10^{-3.3}$
5.	4	-3	$10^{-3.1}$
		-2	$10^{-2.0}$
		-1	$10^{-1.0}$
		0	$10^{1.0}$

Table II. Wear rate for EDMed WC-30Co composite

S.No	Normalized velocity	Normalized pressure	Wear rate
1.	0	-8	$10^{-8.0}$
		-7	$10^{-7.0}$
		-6	$10^{-6.0}$
		-5	$10^{-5.0}$
		-4	$10^{-4.8}$
		-3	$10^{-4.5}$
		-2	$10^{-4.0}$
		-1	$10^{-3.5}$
		0	$10^{-3.0}$
		-8	$10^{-5.0}$
		-7	$10^{-4.5}$
		-6	$10^{-4.3}$
		-5	$10^{-4.1}$
		-4	$10^{-4.0}$
		-3	$10^{-3.5}$

2.	1	-2 -1 0	$10^{-3.2}$ $10^{-3.0}$ $10^{-2.9}$
3.	2	-8 -7 -6 -5 -4 -3 -2 -1 0	$10^{-4.5}$ $10^{-4.0}$ $10^{-3.8}$ $10^{-3.5}$ $10^{-3.4}$ $10^{-3.3}$ $10^{-3.1}$ $10^{-3.0}$ $10^{-2.9}$
4.	3	-8 -7 -6 -5 -4 -3 -2 -1 0	$10^{-4.0}$ $10^{-3.9}$ $10^{-3.8}$ $10^{-3.7}$ $10^{-3.6}$ $10^{-3.5}$ $10^{-3.0}$ $10^{-2.0}$ $10^{1.0}$
5.	4	-8 -7 -6 -5 -4 -3 -2 -1 0	$10^{-4.0}$ $10^{-3.9}$ $10^{-3.7}$ $10^{-3.5}$ $10^{-3.0}$ $10^{-2.5}$ $10^{-2.0}$ $10^{-1.0}$ $10^{1.0}$

The worn-out surfaces are shown in Figure2 and Figure3 and logarithmic values of the experimental results are presented in Table I & Table II.

Normalized wear rate $\tilde{W} = \frac{W}{A_n}$ (1)

W= wear rate, A_n = Nominal contact area

Normalized force $\tilde{F} = \frac{F}{A_n H_0}$ (2)

F=Force, H_o= Room temperature hardness

Normalized Velocity $\tilde{V} = \frac{Vr_o}{a}$ (3)

V= Velocity, r_o= Radius of the nominal contact area, a= thermal diffusivity

B. Probabilistic Neural Network (PNN)

The wear mechanism map was developed by using Probabilistic Neural Network by using the normalized load, normalized speed and normalized wear rate. The map is plotted by taking Normalized velocity on X-axis and Normalized force on Y-axis. The steps involved for the development of wear mechanism map is given below.

- Normalized pressure and velocity is given as an input vector.
- A sample of data points covering the entire mechanism are collected from the numerical wear map.
- MATLAB software is used to design a probabilistic neural network. It creates a two layer network. The first layer has radial basis transfer function neurons. It calculates the layer's output from its net input with the help of a euclidean distance weight function by applying weights to an input to get weighed input. The net input is calculated using a net input function by combining its weighed input and biases. The second layer has competitive transfer function neurons which calculates layer's output from its net input with the help of a dot product weight function by adding weighted input. The net input is calculated using net input function.
- Spread is used to specify the typical distance between input vectors
- Simulation is done by adding the output from two layers corresponding to the class to which it belongs. The output layer neuron produces a binary output value corresponding to highest probability density function and makes the classification decision.

The probabilistic neural net is based on the theory of Bayesian classification and the estimation of probability density functions. It is necessary to classify the input vectors into one of the two classes in a Bayesian optimal manner [10]. This theory allows for a cost function to represent the fact that it may be

worse to misclassify a vector that is actually a member of class "A" than it is to misclassify a vector that belongs to class "B". The Bayes rule is such that the input vector belonging to class "A" is classified as,

$$P_A C_A f_A(x) > P_B C_B f_B(x) \quad (4)$$

where P_A - Priori probability of occurrence of patterns in class "A"

C_A - Cost associated with classifying vectors

$f_A(x)$ - Probability density function of class "A"

Bayes decision rule is applied mainly to estimate the probability density function (PDF). The pdf should be positive all over, should be integrable and the integral over all " x " must be l.

The following estimator is used by the probabilistic neural net to estimate the probability density function. It is given by,

$$f_A(x) = \frac{1}{(2\pi)^{\frac{n}{2}}\sigma^n} - \frac{1}{m_n}\sum_{i=1}^{m_A}\exp\left[-2\frac{(x-x_A)^T(x-x_{AI})}{\sigma^2}\right] \quad (5)$$

where x_{AI} - i[th] training pattern from class "A".

n - Dimension of the input vectors

m_A - Number of training pattern in class "A".

σ -Smoothing parameter (corresponds to standard deviations of Gaussian distribution)

$f_A(x)$ serves as an estimator as long as the probability density function is smooth and continuous, $f_A(x)$ approaches the probability density function as the number of data points used for the estimation increases. It should be noted that the function $f_A(x)$ is a sum of Gaussian distributions. The disadvantage of using this probability density function along with Bayes decision rule is that, the entire training set must be stored and the computation needed to classify an unknown vector is proportional to the size of the training set.

C. Architecture

The architecture of the probabilistic neural net is shown in Figure 4

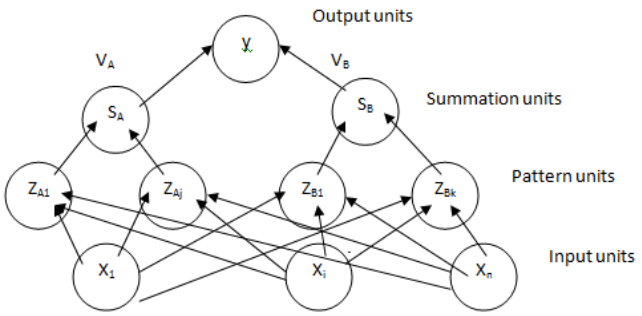

Figure 4. PNN Architecture

The architecture is made up of four types of units

- Input units
- Pattern units-class "A" and class "B"
- Summation units
- Out put units

The weights between the summation unit and the output unit are,

$$V_A = 1$$

$$V_A = -\frac{P_B C_B m_A}{P_A C_A m_b} \quad (6)$$

The bottom units is the input units which represents the "n"input variables (X_1 , X_2 ,...,X_n). The input neurons merely distribute all of the variables X to all neurons in the second units. The pattern unit is fully connected to the input units, with one neurons for each pattern in the training set. The weight values of the neurons in this unit are set equal to the different training patterns. The summation of the exponential term in eqn. (5) is carried out by the summation unit neurons. There is one summation unit neuron for each category. The weights on the connections to the summation units are fixed at unity, so that the summation units simply adds the outputs from the pattern units neurons. Each neuron in the summation units sums the output from the pattern unit neurons, which correspond to the category from which the

training pattern was selected. The output units neurons produces a binary output value corresponding to the highest pdf given by Eqn. (6). This indicates the best classification for that pattern [11].

D. **Training Algorithm**

The training algorithm for the probabilistic neural net is given as,

Step 1: For each training input pattern, $x(p), p = 1.....p$ perform Step 2-3

Step 2: Create pattern unit Z_P :

Weight vector for unit Z_P : $W_P = x(p)$

(unit Zp is either a Z_A unit or Z_B unit)

Step 3: Connect the pattern unit to summation unit. If $x(p)$ belongs to class A, connect pattern unit Z_P to summation unit S_A.

Else, connect pattern unit Z_P to summation unit S_B.

III. DISCUSSION

A. Wear Mechanism Map for WC-30%Co Composite

The volumetric wear rates of the WC-Co are plotted against the logarithmic normalized sliding speed and logarithmic normalized pressure (Figure5). The figure indicates that, at all sliding speeds, the wear rates increased with increase in the applied load. At high sliding speeds, large variations in the slopes of the wear rate curves occurred at a certain load range. The slope changes coincided with the transition from mild wear to severe wear.

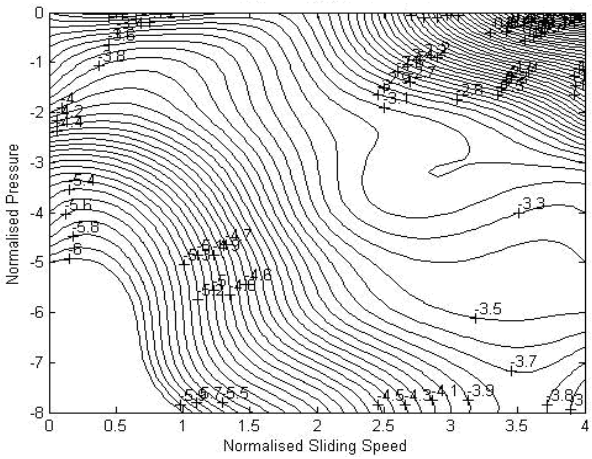

Figure 5. Wear rate map for WC-30Co composite

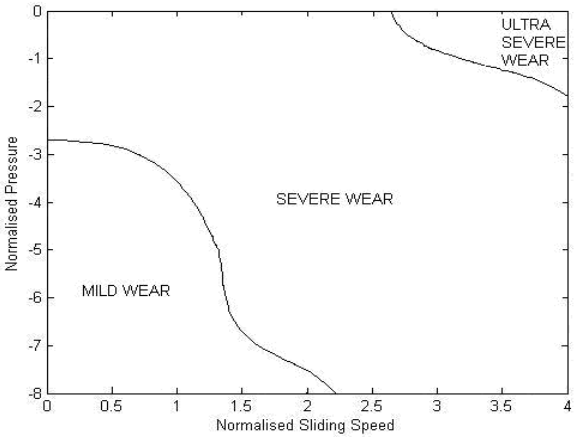

Figure 6. Wear transition map for WC-30Co composite

The wear rates also increased with the applied load, but there was no drastic increase in the slopes of the wear rate versus load curves, i.e. the mild wear regime prevailed until the higher test load. Severe wear is characterized by massive surface damage and production of large 'metallic' debris particles, which are readily identifiable during the test by the naked eye. The onset of severe wear transition to ultra severe wear has been determined during the course of the wear test by visual observation and the differences in debris types are confirmed by the SEM metallographs. As the sliding conditions are changed, the slope of wear rate increased from mild (10^0 - 10^2 to 10^{-8}-10^{-3}) to severe (10^2 - 10^4 to 10^{-2}-10^0) and severe to ultra severe (10^3- 10^4 to 10^{-2}-10^0) and is presented in Figure 6

Wear mechanism map indicates the locations of the dominance of five different wear mechanisms and is shown in Figure 7. Using PNN and the observations on the worn out surfaces, wear mechanism maps are constructed. The different field boundaries on the map suggest where transitions of one dominant wear mechanism to another may take place. The physical wear mechanism maps need extensive physical modeling for determination of boundaries for different mechanisms. In empirical maps, the boundaries are constructed roughly based on the observations of the worm out surface. PNN is comparatively scientific in construction of field boundaries on SEM observations [7]. Because of the wide range of sliding velocity and contact pressure covered by the map, it should enable the designer to decide intelligently whether the material under study will be able to meet the set of requirements for a particular tribological application.

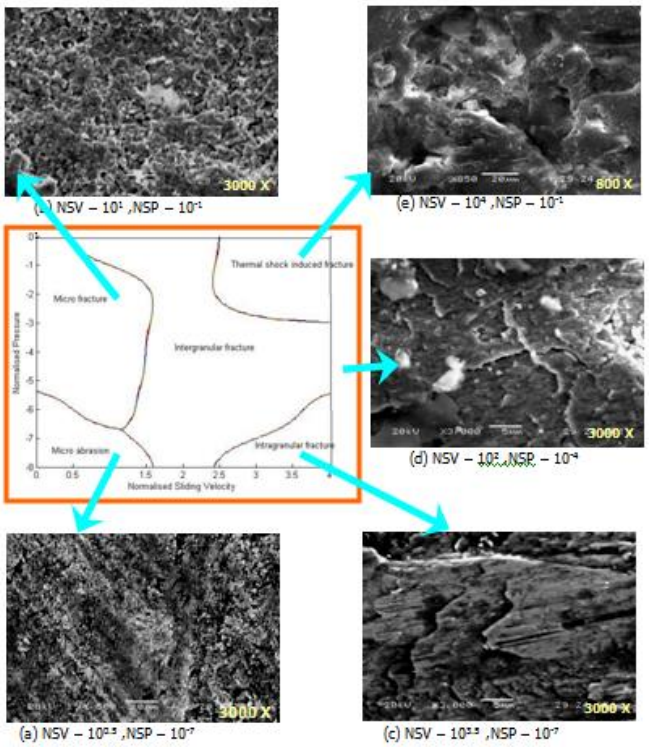

NSV & NSP – Normalized Sliding Velocity & Pressure

Figure 7 : Wear mechanism map forWC-30Co composite

(a) Micro abrasion regime (b) Micro fracture regime (c) Intergranular fracture regime (d) Intragranular fracture regime

(e) Thermal shock induced fracture regime

The micro abrasion wear is observed in the sliding velocity range of 10^0 to $10^{1.5}$ and normalized pressure range of 10^{-8} to 10^{-6}. This wear is due to scratching of hard particles. It usually occurs in systems involving hard particles in motion relative to a surface.it is observed in sem observation of Figure 7(a) The abrasive wear depends critically on the hardness of the abrasive to that of the surface being worn. The worn out surface taken from the mild wear case shows mostly grooves, indicative of micro abrasion being the dominant wear mechanism. Abrasion of the hard metals with the abrasives results in a surface morphology which indicates that wear of the binder phase is more rapid than that of the carbide phase and that carbide pullout is a significant mechanism of wear with these abrasives[12]. Though wear of the carbide particles can be observed, the dominant mechanism of wear is by removal of the binder followed by carbide pullout due to it being undermined. The binder phase can be removed by abrasion by the small abrasive particles, this is in contrast to its removal mechanism with large abrasives which is by extrusion between the carbide grains as the abrasive particles pass over [13]. The worn out surface observed at a normalised sliding

Micro fracture wear is noticed in the normalized sliding velocity range of 10^0 to $10^{1.4}$ and a normalized sliding pressure range of 10^{-5} to 10^0. The worn surface taken from this severe wear regime exhibits evidence of micro fracture and brittle fracture [14]. Brittle fracture has become the dominant wear mechanism in these conditions. The results suggest that significant wear increases as well as change in wear mechanism are associated with this wear transitions. The SEM observation of the worn out surface of the micro fracture at a normalized sliding velocity of 10^1

and normalized pressure of 10^{-2} is shown in Figure7(b).

The intergranular fracture region is identified in the normalized sliding velocity range of $10^{1.5}$ to 10^{4} and in the normalized pressure range of 10^{-8} to 10^{0}. In the case of intergranular fracture, wear particles are generated due to grain chipping or pull-out along the grain boundary [15]. Intergranular fracture will cause removal of grains and severe wear. Pre-existing micro cracks at the grain boundary may preempt the requirements for micro crack nucleation. Their length is proportional to the grain size and is smaller than the radius of the contact area. Intergranular fracture is caused by the propagation of these micro cracks, which may be enhanced by the tensile stress induced by friction [16].For cases of severe abrasive wear involving the coarse abrasives, the mechanism of wear is associated with near surface fractures, initiated primarily from grain boundaries, which caused intergranular cracking and grain pullout [17]. The wear behavior of WC-Co composite shows some micron sized chipping due to intergranular fracture along grain boundaries. The microstructure of the intergranular fracture surface of the specimen slide at the normalized sliding velocity of 10^{2} and the normalized pressure of 10^{-4} is shown in Figure7(c).

The intragranular fracture region is identified at a normalized sliding velocity range of $10^{2.5}$ to10^{4} and a normalized pressure range of 10^{-8} to 10^{-6}. The wear morphology of WC-30Co composites shows the typical abrasive wear with shallow scratches. The wear occurred by brittle fracture and subsurface damage in severe wear regime [18].The shear stress generated a micro crack at the grain boundary and crack propagated through several tungsten carbide grain boundaries. Finally, when the crack reached to the surface, wear debris from several grains is removed. Figure7(d) illustrates the typical intragranular fracture occurred at the normalized sliding velocity of $10^{3.5}$ and the normalized pressure of 10^{-7}.

The thermal shock induced wear is observed in the normalized sliding velocity range of $10^{3.5}$ to 10^{4} at a normalized pressure range of 10^{-2} to 10^{0}. This type of wear is most likely a thermally induced phenomenon due to poor thermal diffusivity in thermal shock induced brittle fracture [19]. SEM observation of thermal shock induced fracture of the worn out surface slide at a normalized velocity of 10^{4} and a pressure of 10^{-1} is illustrated in Figure7(e). In high speed and high load region ultra severe wear occurs and wear mechanisms study suggests gross fracture on the small scale as well as macro fracture .The macro fracture is due to the additional stresses from thermal shock.

It is well known that the rapid temperature changes (thermal shock) can cause serious structural damage to ceramic composites. Thermal shock of ceramics often yields an instantaneous thermal stress, which is, in some case, sufficient to cause considerable cracking damage or even castrophicfailure [20]. The degree of damage and strength degradation of ceramics subjected to severe thermal shock environments are major limiting factors in relation to severe requirements and lifetime performance. Repetitive thermal shock also results in thermal fatigue which has a significant effect on the life of structural components.

B. Wear Mechanism Map for EDMed WC-30Co Composite

The volumetric wear rates of the EDMed WC-30Co are plotted against the normalized sliding speed and normalized pressure (Figure 8). An attempt has been made to study the change in wear behavior of EDMed WC-Co composites. The problem in machining of WC-Co with EDM lies in the differences in melting and evaporation points of the basic elements. Cobalt has easily melted and evaporated from the machined surface. On the other hand, the released grains of tungsten carbide cause instability in machining process because of their gathering and resolidification

in the machined surface, so the surface has micro cracks and craters. The intensity will be increased with pulse energy and the surface roughness value increases [21].

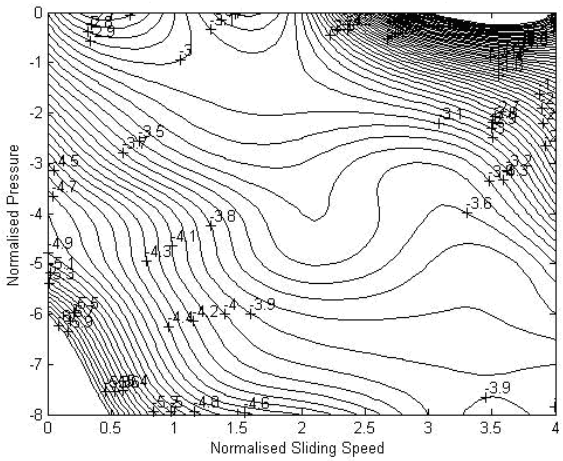

Figure 8 : Wear rate map for EDMedWC-30Co composite

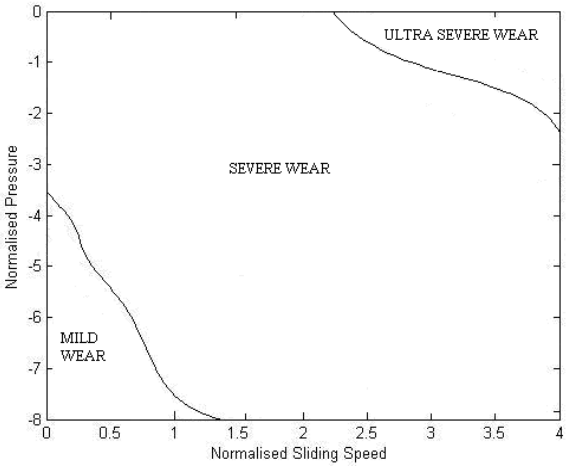

Figure 9 : Wear transition map for EDMed WC-30Co composite

The mild wear regime with increasing Ra, i.e. a decreasing degree of surface finish by EDM, wear depth and initial wear rate increase whereas friction coefficient globally decreases, Severe wear was characterized by massive surface damage due to large shape and size of the crater and thermal spalling, which were readily identifiable during the test by the naked eye. The transition of wear is observed by SEM metalographs. As the sliding conditions are changed, the slope of wear rate increased abruptly from mild (10^{0}- 10^{1} to 10^{-8} - 10^{-4}) to severe ($10^{1.5}$ - 10^{4} to 10^{-4} - 10^{0}) and severe to ultra severe (10^{2} - 10^{4} to 10^{-2} - 10^{0}) and is presented in Figure.9.

Wear maps have been developed to provide guidance with respect to the proper selection of materials and performance envelopes for ceramics. Wear maps also attempts to show the linkage from wear levels, operating conditions and environmental effects to wear mechanisms where constructed. The PNN is used to construct the field boundaries based on SEM observation [7]. Wear mechanism map indicates the locations of the dominance of four different wear mechanisms and is shown in Figure10.

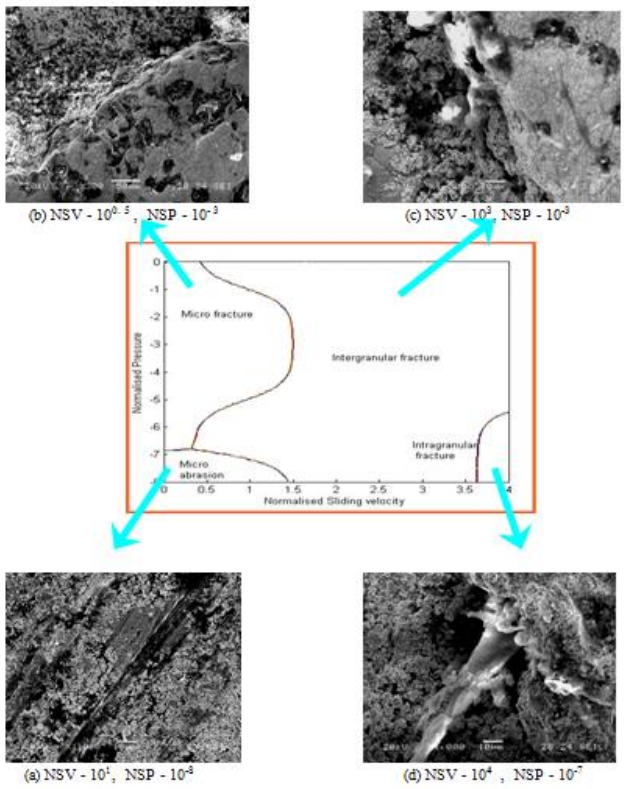

NSV & NSP – Normalized Sliding Velocity & Pressure

Figure 10. Wear mechanism map for EDMedWC-30Co composite

(a) Micro abrasion regime (b) Micro fracture regime (c) Intergranular fracture regime (d) Intragranular fracture regime

The micro abrasion wear is observed in the sliding velocity range of 10^{0} to $10^{1.4}$ and normalized pressure range of 10^{-8} to $10^{-7.}$ This wear is due to scratching of the recast layer which is developed in the EDMed

machined surface of the composites. The surface of EDMed WC-Co parts had the surface recast layer and sub surface heat affected zone, generated by the high local temperature during machining [22]. The worn out surface taken from the mild wear case shows mostly deep scratches, ploughing component (abrasive wear) indicative of micro abrasion being the dominant wear mechanism. The worn out surface observed at a normalised sliding velocity of 10^{1} and sliding pressure 10^{-8} is shown in Figure.10(a).

Micro fracture wear is noticed in the normalized sliding velocity range of 10^{0} to 10^{1} and a normalized sliding pressure range of 10^{-7} to 10^{0}. The worn surface taken from this severe wear regime exhibits evidence of micro fracture and brittle fracture Initial wear rate and friction coefficient are high as the pin penetrates the counter surface, then they decrease till a nearly constant value is reached, corresponding to a regime situation with wear increasing almost linearly with sliding distance, The surface micro cracks and integrity of the machined surfaces are directly related to material removal mechanisms was previously reported. The formation of the craters in EDMed surfaces is due to sparks that form at conductive phase generating melting or possible evaporate and remove the cobalt material[23,24]. The released grains are deposited in the machined surface which leads micro cracks, craters are formed and it will be removed by micro fracture and brittle fracture. The SEM observation of the worn out surface of the micro fracture at a normalized sliding velocity of $10^{0.5}$ and normalized pressure of 10^{-3} is shown in Figure10(b).

The intergranular fracture region is identified in the normalized sliding velocity range of $10^{1.5}$ to 10^{4} and in the normalized pressure range of 10^{-8} to10^{0}. The profiles of the individual transverse sections allow to discern micro structural changes within the recast layer as well as micro cracks running vertically to the shaped surface[25]. These so called longitudinal or radial cracks go well beyond the thermally affected zone into the material. Representative surface morphology of the EDMed surface as observed by SEM, is shown in Figure10(c) The crack propagation through the brittle re-cast layer is probably fairly rapid, but then continues more slowly into the tougher substrate material. The microstructure of the intergranular fracture surface of the specimen slide at the normalized sliding velocity of 10^{3} and the normalized pressure of 10^{-3}.

The intragranular fracture region is identified at a normalized sliding velocity range of $10^{3.6}$ to10^{4} and a normalized pressure range of 10^{-8} to 10^{-6}. The observation of dislodging carbides at the ridges of the tracks would indirectly sustain its presence**.** Under these circumstances, it is speculated that carbides get loosened because of the previous removal of the cobalt binder phase. On the other hand, extensive plastic grooving and moderate to high density of transverse cracks are representative features of contact damage for all the EDM related variants [25]. When the crack reached to the surface, wear debris from several grains was removed. Figure10(d) illustrates the typical intragranular fracture occurred at the normalized sliding velocity of 10^{4} and the normalized pressure of 10^{-7}.

IV. CONCLUSION

The wear mechanism maps are drawn using PNN classification tool. The different wear mechanisms are identified based on SEM observations.

1. The state of ceramic wear is briefly recognized by mild wear, severe wear and ultra sever wear from the view points of wear surface roughness and wear rate. The critical condition for the transition between mild, severe wear and ultra severe wear are given by the certain values of mechanical severity conduct and thermal severity conduct and the ceramic wear map is described with these parameters for the recognition of the mild, severe and ultra severe wear regions.

2. The nature of contour maps, the occurrence of a wear transition can be easily identified on the contour maps as the lines of contact wear rates bunch together to represent a steep ascent. These boundaries then can be plotted to show the locations where the transition occur. There may be one or several transitions with in the speed and load ranges studied in this work, there is usually a mild to severe wear transition and transition from severe wear to ultra severe wear. The locations of these wear transition zones for a given material pair vary within the different speed and different load ranges.
3. Electrical sparks generate craters, bubbles and cracks on the machined surface. Which deteriorates the surface finish and mechanical properties of the EDMed WC-Co surface and should be removed for surface sensitive applications.
4. The thermally induced fracture is fully absent in EDMed wear surface of all three compositions, due to the surface has already subjected to high temperature during machining, so the interfacial temperature has not reached beyond that limit

V. REFERENCE

[1] Pandey.P.C, Shan.H.S (1980), Modern machining processes, Tata McGraw Hill,

[2] Murti.V.S.R, Philip.P.K (1987), " A comparative analysis of machining characteristics in ultrasonic assisted EDM by the response surface methodology", Journal of Production Research, Vol.25, No.2, pp259-272.

[3] McGeough. J.A (1988) Advanced methods of machining, Chapman and Hall..

[4] PriitPodra, Soren Andersson(1997), "Simulating sliding wear with finite element method", Journal of Tribology International, Vol. 32, pp71–81.

[5] Allen,C, Sheen, M, Williams.J, Pugsley.V.A,(2001) "The wear of ultra fine WC-Co hard metals", Journal of Wear, Vol.250, pp604-610.

[6] Hsu.S.M, Ming Shen (2004), "Wear prediction of ceramics", Journal of Wear, Vol. 256, pp867–878.

[7] Lim.S.C,(1998)"Recent developments in wear mechanism maps," Journal ofTribology International, Vol.31, pp87-97.

[8] Lim.S.C, Ashby.M.F (1987)," Wear mechanism maps," Journal ofActa Meta, Vol.35, pp1-24.

[9] Chen.H, Alpas.A.T,(2000) "Sliding wear map for the magnesium alloy Mg-9Al-0.9 Zn (AZ91)", Journal of Wear, Vol. 246, pp106–116.

[10] Sivananthan.S.N, Sumathi.S, Deepa.S.N,(2006) Introduction to neural networks using MATLAB 6.0, Tata McGraw Hill, India.

[11] Berthold. M. R, Diamond.J,(1998) "Constructive training of probabilistic neural networks", Journal ofNeuro computing, Vol. 19, pp167-183.

[12] Lim.S.C,(1998)"Recent developments in wear mechanism maps," Journal ofTribology International, Vol.31, pp87-97.

[13] Mosbah.A.Y, Wexler.D, Calka.A,(2005) " Abrasive wear of WC-FeAl composites", Journal of Wear, Vol.258, pp1337-1341.

[14] Shipway.P.H, Hogg.J.J,(2005) " Dependence of micro scale abrasion mechanisms of WC/Co hard metals on abrasive type", Journal ofWear, Vol. 259, pp44-51.

[15] Koji Kato, KoshiAdachi,(2002) "Wear of advanced ceramics", Journal ofWear, Vol.253, pp1097–1104.

[16] Hsu.S.M ,Shen.M.C, (1996) " Ceramic wear maps", Journal of Wear, Vol. 200, pp154-175.

[17] Adachi.K, Kato.K, Chen.N,(1997) "Wear map of ceramics", Journal of Wear,Vol . 203, pp291-301.

[18] Xiao Feng Zhang, Gun .Y, Lee, Da Chen, Ritchie.R.O, and Lutgard. C, De Jonghe,(2003) "Abrasive wear behavior of heat treated ABC-

silicon carbide", Journal ofAmerican Ceramic Society, Vol. 86, pp1370-78.

[19] Gant.A.J, Gee.M.G, Roebuck.B,(2005) " Rotating wheel abrasion of WC/Co hard metals", Journal of Wear,, Vol. 258, pp178–188.

[20] Gadalla,AM.(1992) " Thermal spalling during electro discharge machining of advanced ceramics and ceramic-ceramic composites". Proceedings of machining of composites materials Symp, ASM, Chicago, pp151-157.

[21] L.Lianes, Idanez.E, Martinez.E, Cases.B, Esteve.J,(2001) "Influence of electrical discharge machining on the sliding contact response of cemented carbides," Journal of Refractory Metals and Hard Materials, Vol.19, pp35-40.

[22] Rajurkar, K. P, Royo.G.F(1989), "Effect of R.F. Control and orbital motion on surface integrity of EDM components", Journal of Mechanical Working Technology, Vol.20, pp341-352.

[23] Jianxin Deng TaichiuLee,(2002) "Effect of ultrasonic surface finishing on the strength and thermal shock behavior of the EDMed ceramic composites", Journal of Machine Tools & Manufacturer, Vol.42, pp245-250.

[24] Bonny.K, De Baets.P,Lauwers.B, Vleugels.J, "Influence of electro discharge machining, micro structural and mechanical properties on wear behavior of hard metals",Department of Mechanical Construction and Production, Laboratory Soete, Ghent University, St.Pietersnieuwstraat 41, B-9000 Ghent, Belgium.

[25] L.Lianes, Idanez.E, Martinez.E, Cases.B, Esteve.J,(2001) "Influence of electrical discharge machining on the sliding contact response of cemented carbides," Journal of Refractory Metals and Hard Materials, Vol.19, pp35-40.